

Landau gauge gluon and ghost propagators at finite temperature from quenched lattice QCD

R. Aouane,¹ V. Bornyakov,² E.-M. Ilgenfritz,³ V. Mitrjushkin,⁴ M. Müller-Preussker,¹ and A. Sternbeck⁵

¹*Humboldt-Universität zu Berlin, Institut für Physik, 12489 Berlin, Germany*

²*Institute for High Energy Physics, 142281, Protvino, Russia*

and Institute of Theoretical and Experimental Physics, 117259 Moscow, Russia

³*Humboldt-Universität zu Berlin, Institut für Physik, 12489 Berlin, Germany*

and Joint Institute for Nuclear Research, VBLHEP, 141980 Dubna, Russia

⁴*Joint Institute for Nuclear Research, BLTF, 141980 Dubna, Russia*

and Institute of Theoretical and Experimental Physics, 117259 Moscow, Russia

⁵*Universität Regensburg, Institut für Theoretische Physik, 93040 Regensburg, Germany*

(Dated: December 31, 2011)

The behavior of the Landau gauge gluon and ghost propagators is studied in pure $SU(3)$ gauge theory at non-zero temperature on the lattice. We concentrate on the momentum range $[0.6, 2.0]$ GeV. For the longitudinal as well as for the transverse component of the gluon propagator we extract the continuum limit. We demonstrate the smallness of finite-size and Gribov-copy effects at temperatures close to the deconfinement phase transition at $T = T_c$ and within the restricted range of momenta. Since the longitudinal component $D_L(q)$ turns out to be most sensitive with respect to the phase transition we propose some combinations of $D_L(q)$ signalling the transition much like “order parameters”.

PACS numbers: 11.15.Ha, 12.38.Gc, 12.38.Aw

Keywords: Lattice gauge theory, non-zero temperature, Landau gauge, ghost and gluon propagators, continuum limit, finite-size effects

I. INTRODUCTION

It is commonly believed that hadronic matter at high temperature undergoes a phase transition into another phase, traditionally called “quark-gluon plasma”. At present, strong efforts are made at RHIC, BNL and at the LHC, CERN to establish undeniable experimental signatures in the final states of heavy-ion collisions indicating that matter had undergone evolution close to or beyond this transition. The existence of such a transition has been concluded long time ago from Hagedorn’s thermodynamical model [1] and later has been one of the first crucial forecasts of lattice QCD (LQCD). The latter uses a formulation of non-Abelian gauge theory which is amenable to ab-initio numerical non-perturbative computations. This formulation also opens the way for analytical calculations at strong and weak coupling. LQCD calculations can provide estimates for the transition temperature, the equation of state close to T_c and above and other features and experimental observables. For a recent review see [2].

In recent years, another powerful non-perturbative approach has been developed based on Dyson-Schwinger equations (DSE) [3–6] and functional renormalization group equations (FRGE) [7, 8]. The main focus was first to find a field theoretical, model-independent description of quark and gluon confinement in terms of the infrared behavior of gauge-variant Green’s functions, in particular of the Landau or Coulomb gauge gluon and ghost propagators. This should allow to confirm or disprove confinement sce-

narios as proposed by Gribov and Zwanziger [9–11] and Kugo and Ojima [12, 13]. Landau gauge gluon and ghost propagators have been intensively studied for zero temperature with DSE and FRGE (see, e.g., [14] and citations therein). On the lattice these propagators have been computed by several groups (see [15, 16] for our own recent computations and references to earlier work by other groups).

If these propagators encode confinement, they should also be considered in LQCD studies at non-vanishing temperature (see [17–20] and for more recent work [21–24]). Complementary to this the temperature dependence has also been studied in the framework of DSE [25–28].

In the recent past we also have extended our lattice computations of the gluon and ghost propagators at zero temperature to the case of non-zero temperature. First results have been obtained without [29] and also with $N_f = 2$ dynamical fermion flavors [30]. In this paper we will focus on results for pure $SU(3)$ gauge theory known to have a first order finite temperature phase transition. We concentrate on the continuum limit within a restricted range of momenta. For this range finite-size or Gribov-copy effects turn out to be small. Moreover, a noticeable sensitivity of the longitudinal component of the gluon propagator with respect to the deconfining phase transition is observed. We show that certain ratios of this component may serve as useful indicators (“order parameters”) for this transition, thus complementing the information obtained from the ever popular Polyakov loop.

The paper is organized as follows. In Section II we

describe the setup of our lattice Monte Carlo simulation. In Section III we review the basic definitions of the gauge-variant propagators on the lattice, modified to finite temperature. In Section IV we present results for the gluon and ghost propagators for various temperatures. The signal of the phase transition is not as strong as one might have expected. Nevertheless, as it is said above, the longitudinal gluon propagator allows us to define ratios which give a clear signal at the deconfinement phase transition. In Sections V and VI we analyze the finite-volume and Gribov-copy effects, respectively. In Section VII we investigate then scaling properties for varying lattice spacing a , keeping the temperature and the volume fixed. This allows us to extrapolate our data to the continuum limit. Finally, in Section VIII, we shall draw our conclusions.

II. SETUP OF THE LATTICE SIMULATIONS

We have generated $SU(3)$ pure gauge field configurations on a four-dimensional lattice of size $N_\sigma^3 \times N_\tau$ with periodic boundary conditions employing standard Monte Carlo simulations using the Euclidean path integral weight $\sim \exp(-S_W)$, where S_W denotes the Wilson one-plaquette action

$$S_W = \beta \sum_{x;\mu>\nu} \left[1 - \frac{1}{3} \Re \text{Tr} \left(U_{x\mu} U_{x+\hat{\mu};\nu} U_{x+\hat{\nu};\mu}^\dagger U_{x\nu}^\dagger \right) \right],$$

$$\beta = 6/g_0^2.$$

g_0 is the bare coupling constant and $U_{x\mu} \in SU(3)$ denotes the link variables. The imaginary-time extent corresponds to the inverse temperature $T^{-1} = N_\tau a$, where $a(\beta)$ is the lattice spacing. For generating the gauge field ensemble we have used the standard hybrid over-relaxation algorithm, with a step of 4 microcanonical over-relaxation sweeps followed by one heatbath step [31, 32]. In both steps a decomposition of $SU(3)$ link variables into $SU(2)$ matrices, as proposed in [33], was applied. $O(2000)$ combined thermalization sweeps were allowed between the individual measurements of the propagators.

In order to determine the temperature dependence of the gluon and ghost propagators, in a first step we kept the lattice spacing fixed (and, as we shall see, sufficiently small) while varying N_τ . As a reference value we have chosen $\beta = 6.337$ providing $a \simeq 0.055$ fm (in accordance with [34]). This β -value corresponds, for $N_\tau = 12$, to a temperature very close to the temperature T_c characteristic for the deconfinement phase transition in a lattice with a linear spatial extent $N_\sigma a(\beta = 6.337) = 48 a \simeq 2.64$ fm. According to Ref. [35] it has been fixed by interpolating with the help of the fit formula

$$\beta_c(N_\tau, N_\sigma) = \beta_c(N_\tau, \infty) - h \left(\frac{N_\tau}{N_\sigma} \right)^3,$$

T/T_c	N_τ	N_σ	β	$a(\text{GeV}^{-1})$	$a(\text{fm})$	n_{conf}	n_{copy}
0.65	18	48	6.337	0.28	0.055	150	1
0.74	16	48	6.337	0.28	0.055	200	1
0.86	14	48	6.337	0.28	0.055	200	1
0.99	12	48	6.337	0.28	0.055	200	1
1.20	10	48	6.337	0.28	0.055	200	1
1.48	8	48	6.337	0.28	0.055	200	1
1.98	6	48	6.337	0.28	0.055	200	1
2.97	4	48	6.337	0.28	0.055	210	1
0.86	8	28	5.972	0.49	0.097	200	27
0.86	12	41	6.230	0.33	0.064	200	1
0.86	16	55	6.440	0.24	0.048	200	1
1.20	6	28	5.994	0.47	0.094	200	27
1.20	8	38	6.180	0.35	0.069	200	1
1.20	12	58	6.490	0.23	0.045	200	1
0.86	14	56	6.337	0.28	0.055	200	1
0.86	14	64	6.337	0.28	0.055	200	1
1.20	10	56	6.337	0.28	0.055	200	1
1.20	10	64	6.337	0.28	0.055	200	1

TABLE I: Temperature values, lattice size parameters, values of the inverse bare coupling β , the lattice spacing a in units of GeV^{-1} and fm, the number n_{conf} of independent lattice field configurations and the number n_{copy} of gauge copies used throughout this study.

where $\beta_c(N_\tau, \infty)$ corresponds to the thermodynamic limit and h denotes a fitted coefficient ($h \lesssim 0.1$). $N_\sigma = 48$ guarantees a reasonable aspect ratio over the whole temperature range $T/T_c \equiv 12/N_\tau \in [12/18, 12/4]$ and permits to reach three-momenta below 1 GeV.

As a second step, we decided to study systematic effects as there are finite-volume effects (cf. Section V), Gribov copy effects (cf. Section VI) and the scaling properties (cf. Section VII) in order to extrapolate to the continuum limit $a \rightarrow 0$ for a couple of momentum values. For the two latter studies we varied $a(\beta)$ while having kept constant the physical spatial volume $(2.7 \text{ fm})^3$ as well as two representative temperature values ($T \simeq 0.86 T_c$ and $T \simeq 1.20 T_c$, respectively).

A compilation of the lattice sizes ($N_\tau \times N_\sigma^3$) and β -values together with the number of independent lattice configurations generated for this study can be found in Table I.

III. GLUON AND GHOST PROPAGATORS

For determining the gluon and ghost propagators we have to fix the gauge. Under local gauge transformations $\{g_x\}$ the link variables transform as

$$U_{x\mu} \xrightarrow{g} U_{x\mu}^g = g_x^\dagger U_{x\mu} g_{x+\hat{\mu}}, \quad g_x \in SU(3). \quad (1)$$

In order to satisfy the Landau gauge transversality condition

$$\nabla_\mu A_\mu = 0 \quad (2)$$

with the lattice gauge potentials

$$A_\mu(x + \hat{\mu}/2) = \frac{1}{2ia g_0} (U_{x\mu} - U_{x\mu}^\dagger) |_{\text{traceless}} \quad (3)$$

it is sufficient to maximize the gauge functional

$$F_U[g] = \frac{1}{3} \sum_{x,\mu} \Re \text{Tr} g_x U_{x\mu} g_{x+\hat{\mu}}^\dagger \quad (4)$$

with respect to g_x . What concerns the Gribov non-uniqueness problem for solutions of the gauge condition Eq. (2) we adopt the strategy of finding gauge copies being as close as possible to the global maximum of $F_U[g]$ [36, 37] as already practiced in [15, 16, 38–41]. This prescription has been shown to provide correct results for Landau gauge photon and fermion propagators within compact $U(1)$ lattice gauge theory [42–45]. Very efficient for this aim is the simulated annealing (SA) algorithm combined with subsequent overrelaxation (OR) iterations [15, 16, 46–48]. The SA algorithm generates gauge transformations $\{g_x\}$ randomly with a statistical weight $\sim \exp(F_U[g]/T_{sa})$. The “temperature” T_{sa} is a technical parameter which is monotonously lowered in the course of 3500 SA simulation sweeps (actually, these are heatbath updates). Also, for better performance, a few microcanonical steps are applied after each heatbath step. In fact, we start with $T_{sa} = 0.45$ and decrease this parameter down to $T_{sa} = 0.01$ in equal steps after each combined sweep. Finally, in order to satisfy the gauge condition Eq. (2) with a local accuracy of

$$\max_x \Re \text{Tr} [\nabla_\mu A_{x\mu} \nabla_\nu A_{x\nu}^\dagger] < \varepsilon, \quad \varepsilon = 10^{-13} \quad (5)$$

we employ the standard OR procedure. Except for the study of the influence of Gribov copies (cf. Section VI), we carry out only one such attempt per configuration to fix the gauge. As in our previous studies, we call the corresponding (first trial) gauge copy “first copy” (*fc*).

The gluon propagator is defined in momentum space as

$$D_{\mu\nu}^{ab}(q) = \left\langle \tilde{A}_\mu^a(k) \tilde{A}_\nu^b(-k) \right\rangle, \quad (6)$$

where $\langle \dots \rangle$ represents the average over configurations, and $\tilde{A}_\mu^a(k)$ denotes the Fourier transform of the gauge-fixed gluon field (3) depending on the integer-valued lattice momentum k_μ ($\mu = 1, \dots, 4$). The latter is related to the physical momentum (for the Wilson plaquette action) as

$$q_\mu(k_\mu) = \frac{2}{a} \sin \left(\frac{\pi k_\mu}{N_\mu} \right), \quad k_\mu \in (-N_\mu/2, N_\mu/2], \quad (7)$$

where $(N_i, i = 1, 2, 3; N_4) \equiv (N_\sigma; N_\tau)$ characterizes the lattice size.

For non-zero temperature it is convenient to split the propagator into two components, the transverse D_T (“chromomagnetic”) (transverse to the heatbath rest frame) and the longitudinal D_L one (“chromoelectric”), respectively,

$$D_{\mu\nu}^{ab}(q) = \delta^{ab} (P_{\mu\nu}^T D_T(q_4^2, \vec{q}^2) + P_{\mu\nu}^L D_L(q_4^2, \vec{q}^2)), \quad (8)$$

where q_4 plays the rôle of the Matsubara frequency, which will be put to zero later on. For the Landau gauge, the tensor structures $P_{\mu\nu}^{T,L}$ represent projectors transverse and longitudinal relative to the ($\mu = 4$)-direction

$$P_{\mu\nu}^T = (1 - \delta_{\mu 4})(1 - \delta_{\nu 4}) \left(\delta_{\mu\nu} - \frac{q_\mu q_\nu}{\vec{q}^2} \right), \quad (9)$$

$$P_{\mu\nu}^L = \left(\delta_{\mu\nu} - \frac{q_\mu q_\nu}{\vec{q}^2} \right) - P_{\mu\nu}^T. \quad (10)$$

For the propagator functions $D_{T,L}$ we find

$$D_T = \frac{1}{2N_g} \left\langle \sum_{i=1}^3 \tilde{A}_i^a(k) \tilde{A}_i^a(-k) - \frac{q_4^2}{\vec{q}^2} \tilde{A}_4^a(k) \tilde{A}_4^a(-k) \right\rangle \quad (11)$$

and

$$D_L = \frac{1}{N_g} \left(1 + \frac{q_4^2}{\vec{q}^2} \right) \left\langle \tilde{A}_4^a(k) \tilde{A}_4^a(-k) \right\rangle, \quad (12)$$

where the number of generators $N_g = N_{\text{color}}^2 - 1$ for $N_{\text{color}} = 3$. The zero-momentum propagator values can be defined as

$$D_T(0) = \frac{1}{3N_g} \sum_{i=1}^3 \left\langle \tilde{A}_i^a(0) \tilde{A}_i^a(0) \right\rangle, \quad (13)$$

$$D_L(0) = \frac{1}{N_g} \left\langle \tilde{A}_4^a(0) \tilde{A}_4^a(0) \right\rangle. \quad (14)$$

Notice that – at least for large enough β – the Landau gauge gluon propagator is expected to depend on the $\mathbf{Z}(3)$ -sectors into which the Polyakov loop spatial averages can fall [49]. Therefore, before carrying out the SA gauge fixing procedure we always apply a $\mathbf{Z}(3)$ -flip as described in Section VI but with respect to the 4-th direction. It ensures the phases of the corresponding Polyakov loop averages to fall into the interval $(-\pi/3, \pi/3]$.

The Landau gauge ghost propagator $G(q)$ and its dressing function $J(q)$ are defined as follows.

$$\begin{aligned} G^{ab}(q) &= a^2 \sum_{x,y} \langle e^{-2\pi i(k/N) \cdot (x-y)} [M^{-1}]_{xy}^{ab} \rangle, \\ &= \delta^{ab} G(q) \equiv \delta^{ab} J(q)/q^2, \end{aligned} \quad (15)$$

where $q^2 \neq 0$ and $(k/N) \cdot (x-y) \equiv \sum_\mu k_\mu (x-y)_\mu / N_\mu$. M denotes the lattice Faddeev-Popov operator corresponding to the gauge field definition (3) and the

related gauge functional (4), i.e.,

$$M_{xy}^{ab} = \sum_{\mu} [A_{x,y}^{ab} \delta_{x,y} - B_{x,y}^{ab} \delta_{x+\hat{\mu},y} - C_{x,\mu}^{ab} \delta_{x-\hat{\mu},y}] \quad (16)$$

with

$$\begin{aligned} A_{x,y}^{ab} &= \Re \text{Tr}[\{T^a, T^b\}(U_{x,\mu} + U_{x-\hat{\mu},\mu})], \\ B_{x,y}^{ab} &= 2 \cdot \Re \text{Tr}[T^b T^a U_{x,\mu}], \\ C_{x,y}^{ab} &= 2 \cdot \Re \text{Tr}[T^a T^b U_{x-\hat{\mu},\mu}], \end{aligned}$$

where T^a ($a = 1, \dots, N_g$) are the Hermitian generators of the $su(3)$ Lie algebra satisfying $\text{Tr}[T^a T^b] = \delta^{ab}/2$. In order to invert M we use the conjugate gradient (CG) algorithm with plane-wave sources $\vec{\psi}_c$ with color and position components $\psi_c^a(x) = \delta_c^a \exp(2\pi i(k/N) \cdot x)$. Actually, we apply a pre-conditioned CG algorithm to solve the equations $M_{xy}^{ab} \phi^b(y) = \psi_c^a(x)$, where as pre-conditioning matrix we use the inverse Laplacian Δ^{-1} with a color-diagonal substructure [50, 51].

In order to study hypercubic lattice artifacts, we have analyzed the influence of the choice of momenta on the behavior of the gluon propagator. When comparing on-axis with diagonal momenta (for $\beta = 6.337$ and in the lower momentum range) we found only small but nonetheless systematic deviations due to the hypercubic lattice geometry. To maximally reduce them the so-called cylinder cut [52]

$$\sum_{\mu} k_{\mu}^2 - \frac{1}{4} (\sum_{\mu} k_{\mu})^2 \leq c, \quad (17)$$

with $k_4 = 0$ and $c = 3$ has been applied to all our data.

IV. RESULTS: GLUON AND GHOST PROPAGATORS VERSUS TEMPERATURE

In Fig. 1 we display the multiplicatively renormalized propagators $D_L(q)$ and $D_T(q)$ as functions of the three-momentum ($q \equiv |\vec{q}|$, $q_4 = 0$) for $\beta = 6.337$, obtained with $N_{\sigma} = 48$ and different N_{τ} , i.e. for temperature values varying from $T = 0.65 T_c$ up to $T \simeq 3 T_c$. For details we refer to the upper section of Table I. The renormalization condition is chosen such that $D_{L,T}$ take their tree level values at the subtraction point $q = \mu$. We choose $\mu = 5$ GeV in order to be close to the perturbative range and still reasonably away from our lattice cutoff ($q_{max} = 2\sqrt{3}/a \simeq 12.4$ GeV).

One can see from Fig. 1 that the temperature dependence of both D_L and D_T becomes weaker with increasing momentum. This weakening proceeds faster for D_T than for D_L . The ultraviolet regions of D_T and D_L turn out to be “phase-insensitive”. This observation was also reported in [30]. More precisely, while the temperature changes from its minimal value

to our maximal one, the change of D_T is less than 5% for $q > 2.2$ GeV, while for D_L this is guaranteed for $q > 2.7$ GeV. For $T \lesssim T_c$ D_L shows a comparatively weak temperature dependence also at small momenta. This changes drastically as soon as $T \gtrsim T_c$. In contrast to that $D_T(q)$ changes monotonously with T in the infrared region. This can be seen in more detail from Fig. 2. There we show the temperature dependence of $D_L(q)$ (left panel) as well as of $D_T(q)$ (right panel) for six selected momenta in the range up to 1.6 GeV.

One can see that D_L at fixed momentum shows strong variations in the neighbourhood of T_c . It is rising with T below T_c and sharply drops around T_c . This behavior looks most pronounced for zero momentum and gets progressively weaker at higher momenta. For the lowest momenta we observe maxima at $T = 0.86 T_c$. It remains open, whether the maxima are shifted away from the transition temperature with increasing volume.¹

In any case, our data confirms that the infrared part of $D_L(p)$ is strongly sensitive to the temperature phase transition [23, 30]. It may serve to construct some kind of order parameters characterizing the onset of the phase transition, as we will propose below. In contrast to that, D_T is ever decreasing and varying smoothly across T_c , showing no visible response to the phase transition at all momenta.

We fit the momentum dependence in the range [0.6 : 8.0] GeV with a Gribov-Stingl interpolation formula [9, 53] used in Refs. [24, 54] and derived later on in the so-called “Refined Gribov-Zwanziger” approach [55, 56]

$$D(q) = \frac{c (1 + d q^{2n})}{(q^2 + r^2)^2 + b^2}. \quad (18)$$

Expected logarithmic corrections needed for the ultraviolet limit have been neglected here (for a thorough discussion see [52]). We put throughout $n = 1$. In a first attempt we have left b varying. We obtained values compatible with $b = 0$ except for $D_T(q)$ at the highest three temperature values inspected. Therefore, in all other cases we have repeated the fits with fixed $b = 0$ and obtained χ_{df}^2 -values reasonably below 2.0. The fit parameters can be found in Table II.² Since we expect to see a plateau and even a bend over for D_T at momenta below our minimal ones the parameter b might become nonzero also at lower temperatures. This would then correspond to a complex effective mass parameter.

¹ For $SU(2)$ gauge theory the maximum of $D_L(0)$ was recently reported [24] to move away from the transition with decreasing lattice spacing.

² Note that for $b = 0$ Eq. (18) is equivalent to the interpolation formula $D(q) = \frac{\gamma}{(q^2 + \delta^2)^2} + \frac{\beta}{(q^2 + \delta^2)^2}$.

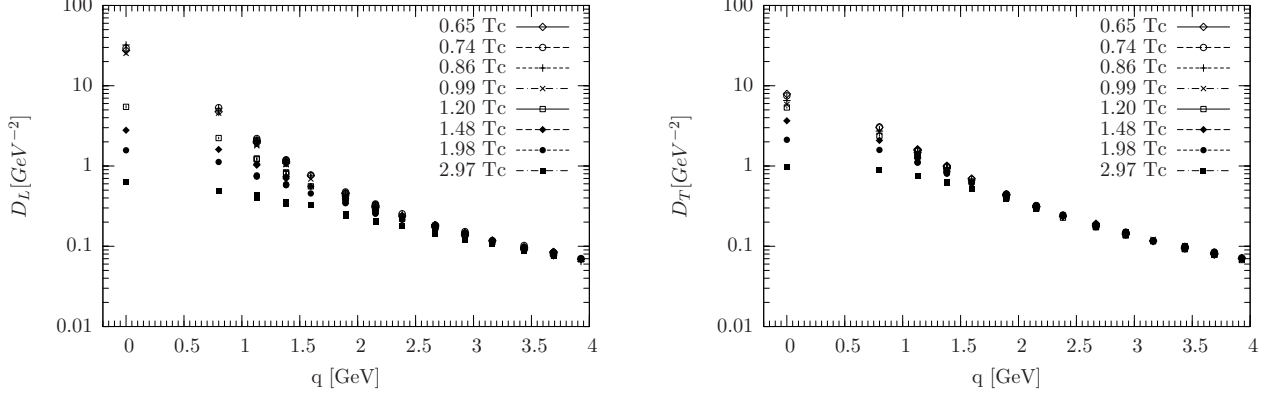


FIG. 1: Temperature dependence of the longitudinal (l.h.s.) and the transverse (r.h.s.) gluon propagator for $\beta = 6.337$ and a spatial lattice size $N_\sigma = 48$.

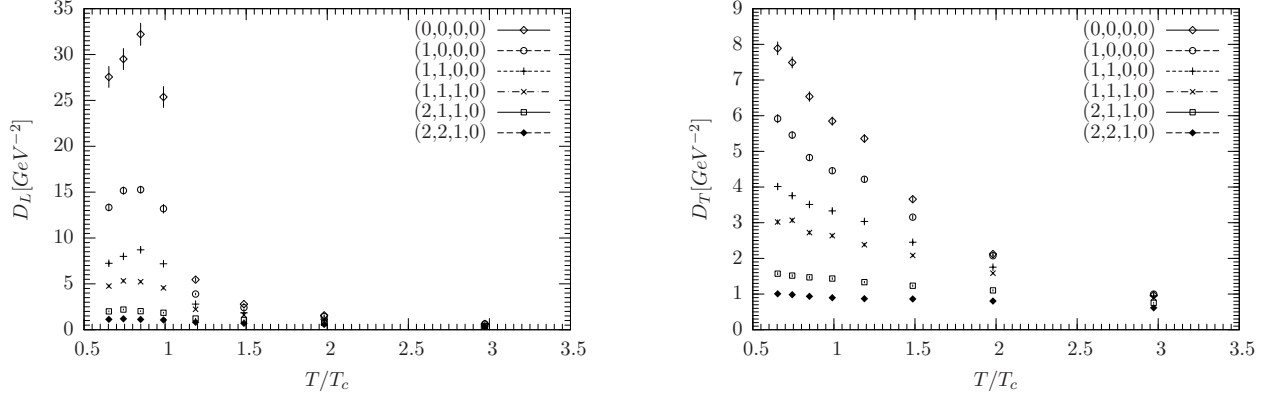


FIG. 2: The longitudinal propagator, D_L , (l.h.s.) and the transverse one, D_T , (r.h.s.) vs. temperature for a few low momenta, the latter represented as (k_1, k_2, k_3, k_4) . $\beta = 6.337$ and $N_\sigma = 48$.

We have tried to form quantities constructed from the gluon propagator which can serve as indicators for the deconfinement transition. First, we plot the ratio

$$\chi = [D_L(0, T) - D_L(q, T)] / D_L(0, T) \quad (19)$$

as a function of T/T_c in the left panel of Fig. 3. We observe that all the curves labelled by the momentum 4-tuples in the legend show approximate plateaux below T_c . Then, passing the phase transition they suddenly fall off with slopes becoming slightly smaller with increasing momentum, but still with visible temperature sensitivity. This means that χ can be used as an indicator for the deconfinement transition and, moreover, the transition can be traced even at rather high momentum. This was not so clear from the l.h.s. of Fig. 2, where the behavior of D_L at higher momenta looks rather smooth.

From the behavior of χ , at least in the interval $0.65 T_c \lesssim T \lesssim T_c$ and at low momentum, one can conjecture the factorization

$$D_L(q; T) \simeq A(q) \cdot B(T). \quad (20)$$

Then, as long as the temperature T varies in the given interval, the change of D_L can be described by a momentum independent rescaling. This is a rather non-trivial property from which further conclusions can be drawn. For example, in the interpolation formula (18) above, we should find the mass parameter r^2 and the parameter d to be (approximately) temperature independent as long as $T < T_c$.

From the left panel of Table II one can see that this is true for the parameter d which varies within error bars. The variation of parameter r^2 is up to 30%. This comparatively large variation might be explained by the fact that the propagators were fitted over a wide range of momenta, specifically from 0.6 to 8 GeV, while the factorization we expect to hold only at low momenta. Indeed, a fit in the range up to 2.5 GeV which includes also the zero momentum value has shown r^2 to become approximately constant. It remains to be seen, whether this behavior in the infrared region survives the continuum and the thermodynamic limites which goes beyond the scope of this paper.

Parameters		D_L fits					D_T fits				
T/T_c	N_τ	$r^2(\text{GeV}^2)$	$b(\text{GeV}^2)$	$d(\text{GeV}^{-2})$	$c(\text{GeV}^2)$	χ^2_{df}	$r^2(\text{GeV}^2)$	$b(\text{GeV}^2)$	$d(\text{GeV}^{-2})$	$c(\text{GeV}^2)$	χ^2_{df}
0.65	18	0.372(29)	0.0	0.192(8)	4.29(17)	1.49	0.751(24)	0.0	0.153(4)	5.40(14)	1.17
0.74	16	0.296(22)	0.0	0.206(7)	4.11(13)	1.40	0.756(20)	0.0	0.161(3)	5.31(11)	0.99
0.86	14	0.257(22)	0.0	0.221(8)	3.70(13)	1.57	0.847(22)	0.0	0.152(4)	5.50(12)	1.09
0.99	12	0.359(30)	0.0	0.209(10)	3.89(16)	1.83	0.869(26)	0.0	0.157(4)	5.45(14)	1.44
1.20	10	1.029(41)	0.0	0.155(6)	5.43(21)	1.27	0.951(25)	0.0	0.147(4)	5.56(13)	1.17
1.48	8	1.547(47)	0.0	0.118(4)	7.12(24)	1.06	0.886(138)	0.810(167)	0.146(11)	5.70(42)	1.46
1.98	6	2.455(75)	0.0	0.086(4)	9.55(37)	1.35	0.856(109)	1.398(62)	0.133(8)	6.15(34)	0.93
2.97	4	5.327(159)	0.0	0.045(2)	17.15(73)	0.51	0.927(126)	2.559(33)	0.100(6)	7.58(41)	1.01

TABLE II: Results from fits with Eq. (18) ($n = 1$) for D_L (l.h.s.) and D_T (r.h.s.) corresponding to the Monte Carlo data shown in Fig. 1 ($\beta = 6.337$, $N_\sigma = 48$). The fit range is $[0.6 : 8.0]$ GeV. The values in parentheses provide the fit errors. The boldface printed b -values indicate that they are fixed to zero.

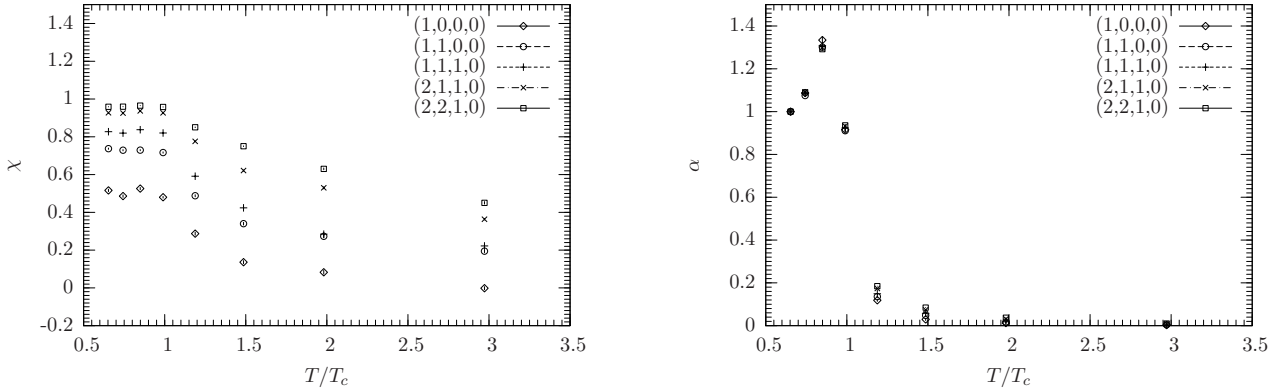


FIG. 3: Temperature behavior of the ratios χ (Eq. (19), left panel) and α (Eq. (21), right panel) at low momenta as given in the legend, for a spatial lattice size $N_\sigma = 48$ and $\beta = 6.337$.

Let us consider another ratio

$$\alpha = \frac{D_L(0, T) - D_L(q, T)}{D_L(0, T_{min}) - D_L(q, T_{min})}, \quad T_{min} = 0.65 T_c, \quad (21)$$

which according to the factorization (20) should be approximately momentum independent. Indeed, this can be seen from the right panel of Fig. 3. Moreover, $\alpha(q, T)$ should resemble qualitatively the temperature dependence of D_L at $q = 0$. Close to T_c , however, α falls off reaching very small values at higher temperatures (around $2 T_c$). Therefore, we conclude that both quantities χ (ceasing to be constant) and α (with its strong fall off) signal the finite-temperature transition. It remains to be seen, whether they also map out the (pseudo)critical behavior in unquenched QCD.

Let us note that our volumes are not large enough to study the infrared asymptotic behavior. Moreover, at the lowest momenta we expect systematic deviations due to finite-size effects, lattice artifacts, and Gribov copy effects. This concerns also the parameters χ and α because of their dependence on the value $D_L(q = 0)$. The systematic effects will be discussed to some extent in Sections V to VII, in order to identify the

momentum range, where they play only a negligible rôle.

Summarizing, in agreement with findings in other recent investigations [21–24, 30] we observe the strongest response to the phase transition to occur in the gluonic chromoelectric sector (the longitudinal propagator) rather than in the gluonic chromomagnetic one (the transverse propagator).

We have also computed the ghost propagator according to Eq. (15), restricting it for simplicity to the diagonal three-momenta and vanishing Matsubara frequency, $k_\mu = (k, k, k, 0)$ with $k = 1, \dots, 7$. The data are again normalized at $\mu = 5$ GeV, such that the ghost dressing function equals unity at $q = \mu$. The result for the latter function is displayed in Fig. 4. In comparison with the gluon propagator we see the ghost propagator to change relatively weakly with the temperature.³ This is in agreement with the observation in [21]. An increase becomes visible at tempera-

³ Note the use of a linear scale at the vertical axis in Fig. 4a in contrast to the logarithmic one in Fig. 1.

ture values $T > 1.4T_c$ for the lowest momenta studied (see Fig. 4b). The relative insensitivity with respect to the temperature is the reason why we will not further consider the ghost propagator in what follows.

V. FINITE-VOLUME EFFECTS

In order to estimate finite-volume effects we compare the data shown before with data obtained on even larger spatial volumes while keeping fixed the coupling (at $\beta = 6.337$) and two temperature values, $T = 0.86 T_c$ (confinement) and $T = 1.2 T_c$ (deconfinement), respectively. The linear spatial extent varies from $48a = 2.64 \text{ fm}$ to $64a = 3.52 \text{ fm}$ (see also the middle section in Table I).

In Figs. 5 and 6 we show the corresponding plots for D_L and D_T , respectively. In all four cases we observe the effects to be small for momenta above 0.6 GeV .⁴ For lower momenta, especially at zero momentum, systematic deviations become more visible. With increasing volume the infrared values of D_L seem to rise, whereas for D_T the opposite is the case. This behavior has already been reported for pure gauge theories in [29, 57] for $SU(2)$ and in [30] for $SU(3)$, respectively.

VI. GRIBOV COPY EFFECTS

In order to study Gribov copy effects we compare “first”, i.e. randomly occurring copies (fc) with “best” copies (bc). The latter were produced as follows.

We searched for copies within all $3^3 = 27$ $\mathbf{Z}(3)$ sectors characterized by the phase of the spatial Polyakov loops, i.e. Polyakov loops in one of the three spatial directions. For this purpose the $\mathbf{Z}(3)$ flipping operations [30, 40] were carried out on all link variables $U_{x,i}$ ($i = 1, 2, 3$) attached and orthogonal to a 3d hyperplane with fixed x_i by multiplying them with $\exp\{\pm 2\pi i/3\}$. Such global flips are equivalent to non-periodic gauge transformations and do not change the pure gauge action. For the 4th direction, we stick to the sector with $|\arg P| < \pi/3$ which provides maximal values of the functional (4) at the β -values considered in this section [30]. Thus, the flip operations combine for each lattice field configuration the 27 distinct gauge orbits of strictly periodic gauge transformations into one larger gauge orbit.

The number of copies actually considered in each of the 27 sectors depends on the rate of convergence (with increasing number of investigated copies) of the

propagator values assigned to the best copy, in particular at zero momentum. From our experience with $SU(3)$ theory [30] we expect that the effect of considering gauge copies in different flip-sectors is more important than probing additional gauge copies in each sector. For this reason and to save CPU time we have considered one gauge copy for every $\mathbf{Z}(3)$ -sector; therefore, in total $n_{copy} = 27$ gauge copies for every configuration.

To each copy the simulated annealing algorithm with consecutive overrelaxation was applied in order to fix the gauge. We take the copy with maximal value of the functional (4) as our best realization of the global maximum and denote it as best (“ bc ”) copy.

The parameters of the SA algorithm in the study of Gribov copies were slightly different from those described above in Section III. 2000 SA combined simulation sweeps with a ratio 11:1 between microcanonical and heat bath sweeps were applied starting with $T_{sa} = 0.5$ and ending at $T_{sa} = 0.0033$.

Since this procedure is quite CPU time consuming we restricted this investigation to coarser lattices 6×28^3 and 8×28^3 with larger lattice spacing, such that both the temperature values $T = 0.86 T_c$ and $T = 1.20 T_c$, respectively, as well as the physical 3d volume $(2.64 \text{ fm})^3$ were approximately reproduced.

In Figs. 7 and 8 we compare bc with fc results for the gluon propagators D_L and D_T , respectively. As one can see, D_L is almost insensitive to the choice of Gribov copies (at least, for the comparatively small values of N_τ we consider), as has been already reported in [29] for the $SU(2)$ case and in [30] for the $SU(3)$ case. On the contrary, the transverse propagator is strongly affected in the infrared region. This observation is independent of the temperature. Moreover, we see that the transverse gluon propagator values in the infrared become lowered for bc compared with fc results. These observations resemble those made already in [29] and [30].

The main conclusion of this section is that Gribov copy effects may be neglected for all nonzero momenta in the case of the longitudinal propagator (at least, for comparatively small values of N_τ), and for momenta above 800 MeV in the case of the transverse propagator. The momentum range where the last statement is true might depend on the temperature.

VII. SCALING AND CONTINUUM LIMIT

In order to check for good scaling properties we have used the same reference values for the temperature below and above T_c as discussed before (i.e., $0.86 T_c$ and $1.20 T_c$). We kept also the spatial volume fixed at $(2.7 \text{ fm})^3$. We compare the renormalized propagators at four different values for the lattice spacing $a(\beta)$ (see Table I). Our results are displayed for the momentum

⁴ Below T_c the transverse propagator changes by less than 12 %, the longitudinal one by less than 5 %. Above T_c the transverse propagator varies by less than 8 % and the longitudinal one by less than 11 %.

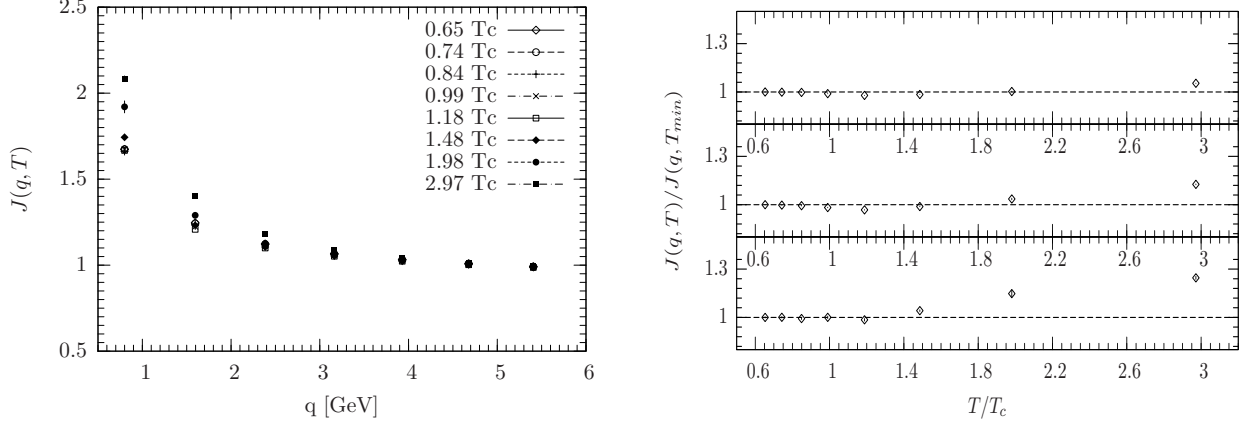


FIG. 4: The renormalized ghost dressing function $J(q, T)$ for various temperature values (l.h.s.) and its dependence on the temperature shown for the fixed diagonal 3-momenta $((k, k, k, 0), k = 1, 2, 3)$ and normalized with $J(q, T_{min})$ for $T_{min} = 0.65T_c$ (r.h.s.). The lowest panel shows the lowest momentum. All data are obtained at $\beta = 6.337$ on a lattice with spatial size $N_\sigma = 48$.

range up to 1.5 GeV in Fig. 9 for D_L and in Fig. 10 for D_T , respectively. Gauge fixing has been carried out as originally described in Section III.

We provide the renormalization factors for

$$D_{L,T}(q, \mu) \equiv Z_{L,T}(a, \mu) D_{L,T}^{bare}(q, a) \quad (22)$$

in the left panel of Table III. As expected the Z -factors of D_L and D_T approximately agree.

From Figs. 9 and 10 we see that the scaling violations happen to be reasonably small for momenta above 0.8 GeV. This shows that our choice of $a = 0.055$ fm for $\beta = 6.337$ was already close to the continuum limit.

In order to study the a -dependence at five particular physical momenta p we need interpolations of the momentum dependence in between the data points. For the fit within the interval $0.6 \text{ GeV} \leq q \leq 3.0 \text{ GeV}$ we have used again Eq. (18) with parameter b fixed to zero. The values of the fit parameters are displayed in the right hand panels of Table III. In all cases we find χ^2 -values per degree of freedom around or below unity.

The propagators, now interpolated to the set of selected momentum values, are shown in Fig. 11 for D_L and in Fig. 12 for D_T , respectively, as functions of the lattice spacing a . We show them together with the respective fit curves

$$D(a; p) = D_0 + B \cdot a^2 \quad (23)$$

assuming only $O(a^2)$ lattice artifacts. The corresponding fit results are collected in Table IV. The respective fit parameters D_0 represent the continuum limit values of the propagators at the preselected momenta.

Our lattice propagator data obtained for $\beta = 6.337$ as discussed in Section IV can now be compared with

the values extrapolated to the continuum limit. This is shown in Fig. 13. In more detail, we can compare the continuum extrapolated values at some lower momentum – say at $q = 0.70$ GeV – with those obtained from $a(\beta = 6.337) = 0.055$ fm and interpolated to the same momentum. Then we find deviations being smaller than 4%. Thus, we are really justified to say that the results obtained for $\beta = 6.337$ in the given momentum range are already very close to the continuum limit. The continuum limit extrapolated propagators can be easily interpolated with formula Eq. (18). The results are drawn in Fig. 14.

We conclude that for the higher β -values and the momentum range considered in this paper we are close to the continuum limit. Moreover, systematic effects as there are finite-volume and Gribov copy effects seem to be negligible for momenta above 0.8 GeV.

VIII. CONCLUSIONS

We have presented lattice results for the Landau gauge gluon and ghost propagators computed in pure gauge $SU(3)$ lattice theory at non-zero temperatures.

Overall, our results agree with those published in [23] and there are hardly any deviations which are not due to the lattice discretization or the finite volume. However, our aim here was to go a step further and to provide results in the continuum limit for temperatures below and above the deconfinement phase transition, and this with negligible systematic finite-volume and Gribov copy effects. For this to become feasible we had to restrict the analysis to a well-defined momentum range around 1 GeV.

The systematic effects were studied at two temperatures, $T = 0.86T_c$ and $T = 1.20T_c$, such that we cannot really tell, what happens very close to T_c . Since

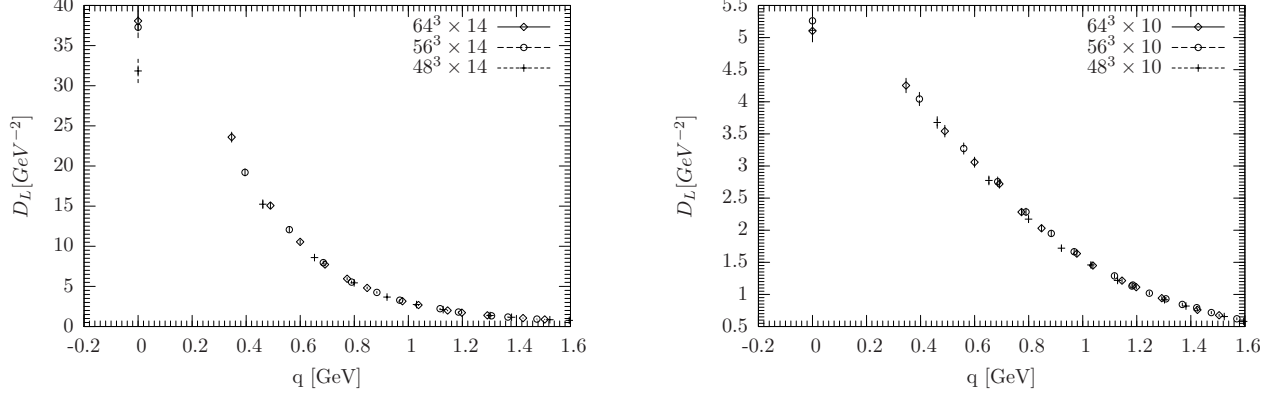


FIG. 5: Finite-size effect study for D_L at $\beta = 6.337$. l.h.s.: $T = 0.86 T_c$, r.h.s.: $T = 1.20 T_c$.

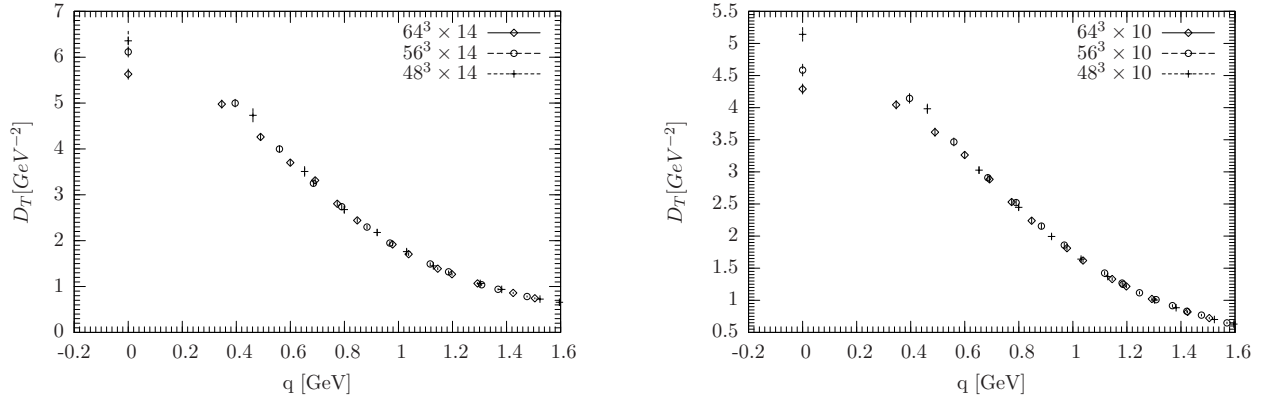


FIG. 6: Same as in Fig. 5 but for D_T .

Parameters				Z-factors	
T/T_c	β	N_σ	N_τ	Z_T	Z_L
0.86	5.972	28	8	1.43	1.43
0.86	6.230	42	12	1.45	1.47
0.86	6.337	48	14	1.48	1.53
0.86	6.440	56	16	1.64	1.66
1.20	5.994	28	6	1.46	1.46
1.20	6.180	38	8	1.52	1.52
1.20	6.337	48	10	1.62	1.63
1.20	6.490	58	12	1.62	1.65

D_L fits			
$r^2(\text{GeV}^2)$	$d(\text{GeV}^{-2})$	$c(\text{GeV}^2)$	χ^2_{df}
0.317(20)	0.138(24)	4.67(26)	0.30
0.254(9)	0.224(7)	3.90(8)	0.44
0.262(12)	0.224(11)	3.80(12)	0.42
0.256(7)	0.220(6)	3.86(7)	0.24
0.995(37)	0.153(10)	5.46(24)	0.80
0.985(20)	0.163(6)	5.34(13)	0.28
0.960(19)	0.180(7)	4.96(13)	0.22
1.018(18)	0.162(5)	5.27(11)	0.06

D_T fits			
$r^2(\text{GeV}^2)$	$d(\text{GeV}^{-2})$	$c(\text{GeV}^2)$	χ^2_{df}
0.810(23)	0.148(7)	5.49(17)	1.19
0.835(16)	0.151(5)	5.69(12)	0.52
0.867(18)	0.142(6)	5.62(14)	0.14
0.880(15)	0.143(4)	5.65(11)	0.36
0.894(26)	0.144(7)	5.55(18)	1.10
0.924(22)	0.142(6)	5.71(16)	0.57
0.982(27)	0.133(8)	5.87(21)	0.59
0.963(19)	0.140(5)	5.77(13)	0.45

TABLE III: **Left panel:** Renormalization factors $Z_{L,T}$ of the renormalized propagators $D_{T,L}(q, \mu)$ according to Eq. (22). The renormalization point is $\mu = 5$ GeV. **Right panels:** Fit parameters and χ^2_{df} for fits of D_L (l.h.s.) and D_T (r.h.s.) using the generic fit function $D(q^2)$ acc. to Eq. (18), but with $b = 0$. The fit range is restricted to $[0.6 : 3.0]$ GeV. The fit errors are indicated in parentheses.

for our reference value $\beta = 6.337$ the critical temperature T_c is reached with $N_\tau = 12$, there is hope that also in this case we keep close to the continuum limit and the other systematic effects are under control.

Our results and their parametrization can be further used to compare with the outcome of Dyson-Schwinger or functional renormalization group equa-

tions for the gluon propagators or employed as reliable input in Dyson-Schwinger studies of the quark propagator. It is well-known that the non-perturbative continuum approaches rely on a truncated tower of equations for the propagators and vertex functions. The way of how it is truncated has a strong influence on the behavior, especially at intermediate momenta.

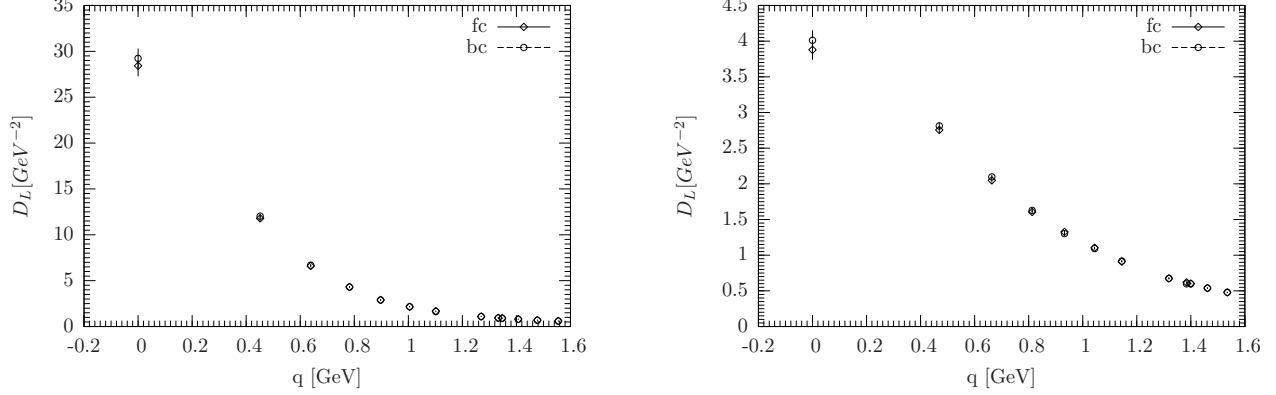


FIG. 7: Comparison of the bc with the fc Gribov copy result for the longitudinal propagator D_L (unrenormalized) (l.h.s.: $T = 0.86 T_c$, r.h.s.: $T = 1.20 T_c$).

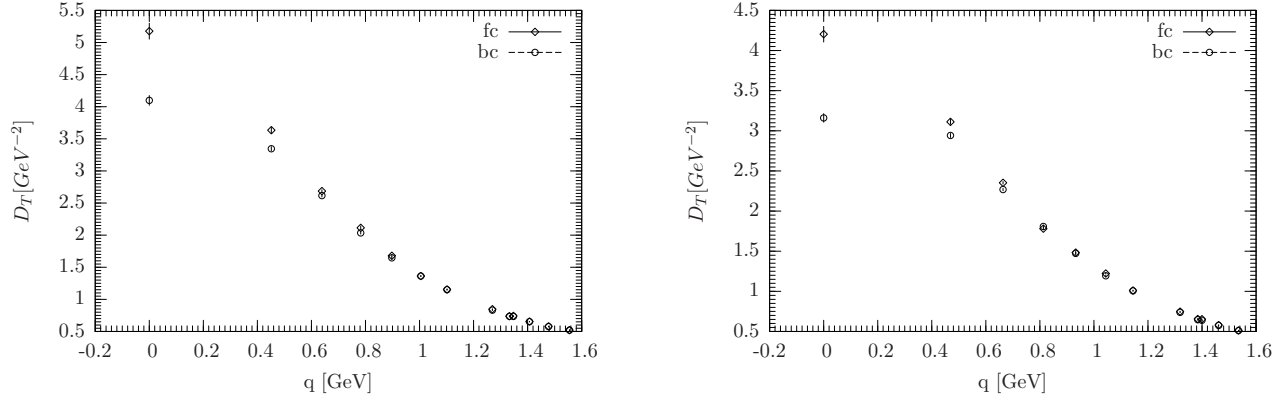


FIG. 8: Same as in Fig. 7 but for the transverse propagator D_T (l.h.s.: $T = 0.86 T_c$, r.h.s.: $T = 1.20 T_c$).

Parameters		D_L fits		D_T fits	
T/T_c	$p(\text{GeV})$	B	$D_0(\text{GeV}^{-2})$	B	$D_0(\text{GeV}^{-2})$
0.86	0.70	-1.3(28.1)	7.68(16)	32.3(20.0)	3.20(11)
0.86	0.85	13.5(14.5)	4.63(8)	19.5(14.0)	2.42(8)
0.86	1.00	12.3(7.9)	2.95(4)	11.7(9.8)	1.83(5)
0.86	1.20	7.0(4.1)	1.75(2)	5.9(6.4)	1.27(4)
0.86	1.40	3.0(2.6)	1.12(1)	3.2(4.4)	0.90(2)
1.20	0.70	23.1(9.3)	2.48(5)	30.7(11.0)	2.84(6)
1.20	0.85	15.8(6.5)	1.93(4)	18.5(7.4)	2.19(4)
1.20	1.00	11.8(4.7)	1.49(2)	10.8(4.8)	1.68(2)
1.20	1.20	7.4(3.3)	1.07(2)	5.3(3.0)	1.19(2)
1.20	1.40	4.8(2.2)	0.77(1)	2.4(1.8)	0.86(1)

TABLE IV: Results of the fits for D_L (l.h.s.) and D_T (r.h.s.) as a function of the lattice spacing a using the fit function $D(a; p)$ acc. to Eq. (23). The errors of the fit parameters are given in parentheses. χ^2_{df} in all cases is close or well below unity. See also Figs. 11 and 12.

Lattice results from first principles as those presented here can help to tune the truncation correspondingly.

Concentrating on this aim we have been forced to choose the lattice spacing a and the linear spatial lattice extent N_σ such that we were prevented from going

far towards the infrared limit. Therefore, we were not able to clarify the question, what the correct behavior is in the far infrared region. Concerning this region we know, that the Gribov problem is serious and still not completely understood. This is also the reason,

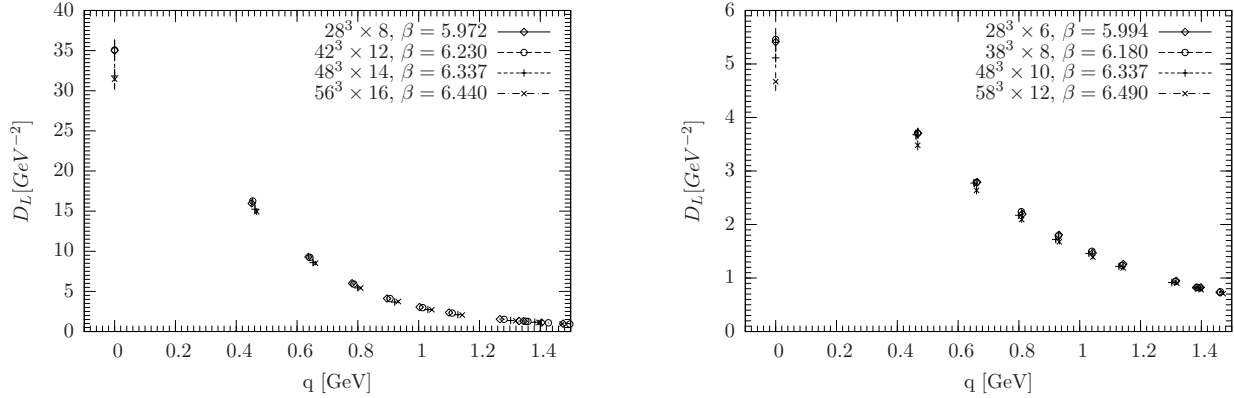


FIG. 9: The longitudinal propagator D_L , renormalized at $\mu = 5$ GeV, obtained for fixed physical volume and temperature but varying $a = a(\beta)$. l.h.s.: $T = 0.86 T_c$, r.h.s.: $T = 1.20 T_c$.

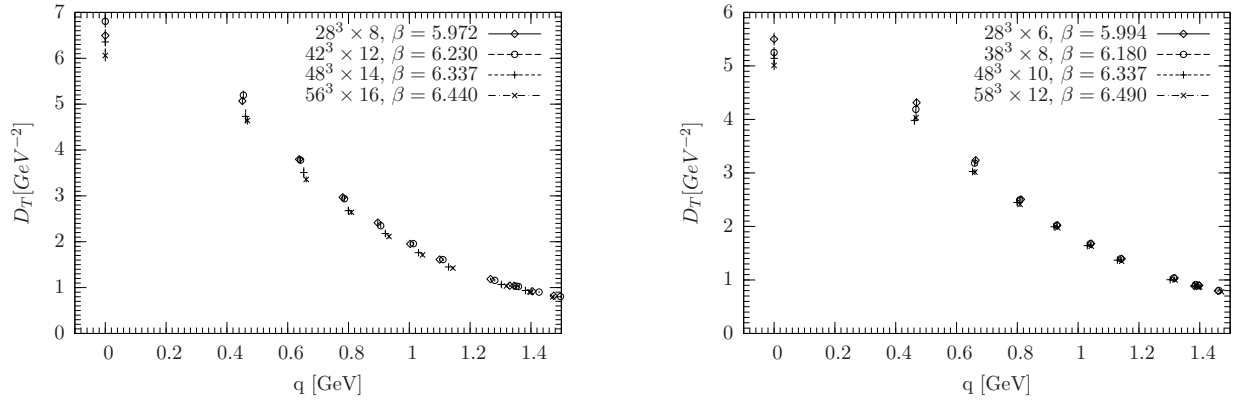


FIG. 10: Same as in Fig. 9 but for the transverse propagator D_T . l.h.s.: $T = 0.86 T_c$, r.h.s.: $T = 1.20 T_c$

why we did not try in this paper to give estimates for the color-electric and -magnetic screening masses.

Our results confirm that, contrary to the transverse gluon propagator D_T and to the ghost propagator G , the longitudinal gluon propagator D_L is sensitive to the deconfinement transition. However, despite of the fact that we are faced with a first order phase transition the response to it occurs relatively smooth. We were able to propose two parameters built from D_L which can be employed as indicators (kind of “order parameters”) for the transition itself. One might hope that they will help to shed additional light on the transition region also in full QCD. There, at least for $N_f = 2$ quark flavours within the range of intermediate pion masses a rather smooth crossover is expected (see e.g. [2] and references therein, as well as [58, 59]). We shall come back to this question in the near future.

Acknowledgments

We acknowledge useful discussions with F. Burger,

C. Fischer, A. Maas, T. Mendes, J. Pawłowski, and L. von Smekal. R. A. gratefully acknowledges financial support by the Yousef Jameel Foundation, A. S. from the European Reintegration Grant (FP7-PEOPLE-2009-RG No.256594), V.K.M. and M.M.-P. by the Heisenberg-Landau program agreed upon between JINR and the German BMBF, V.B. by the Federal Programme Cadres of the Russian Ministry of Science and Education as well as by the grants RFBR 09-02-00338-a and NSh-6260.2010.2. We thank the HLRN Berlin-Hannover and the JINR Computing Center for generous supply with computing time.

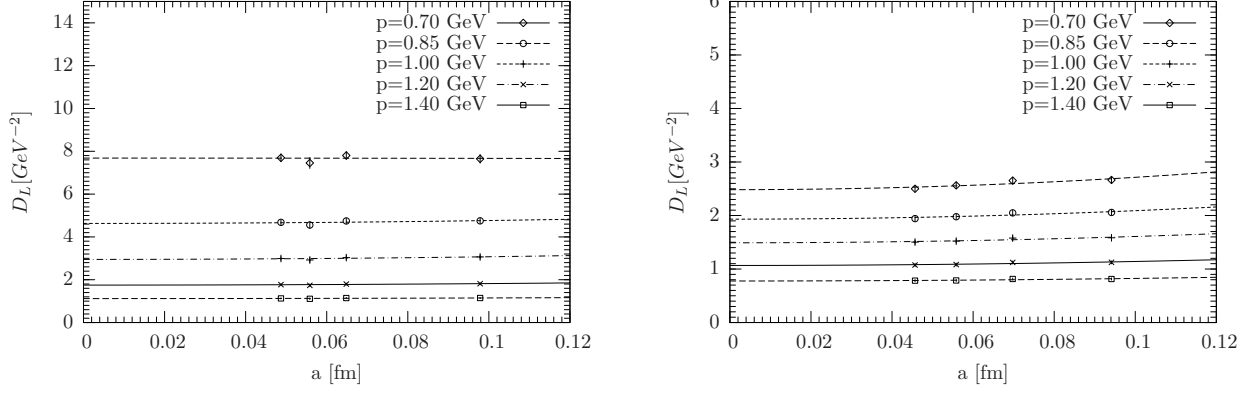


FIG. 11: D_L vs. lattice spacing a for a set of different preselected momenta p . l.h.s. $T = 0.86 T_c$; r.h.s. $T = 1.20 T_c$.

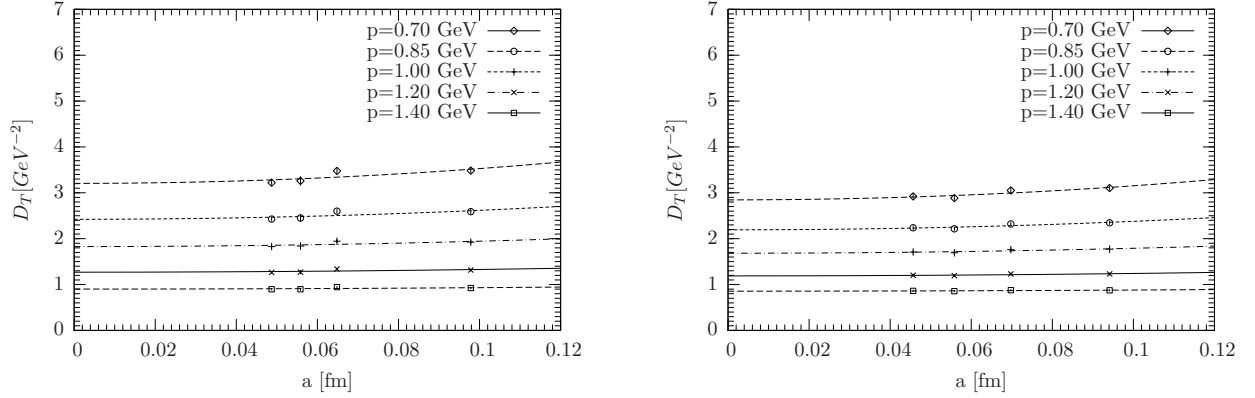


FIG. 12: Same as in Fig. 11 but for D_T . l.h.s. $T = 0.86 T_c$; r.h.s. $T = 1.20 T_c$.

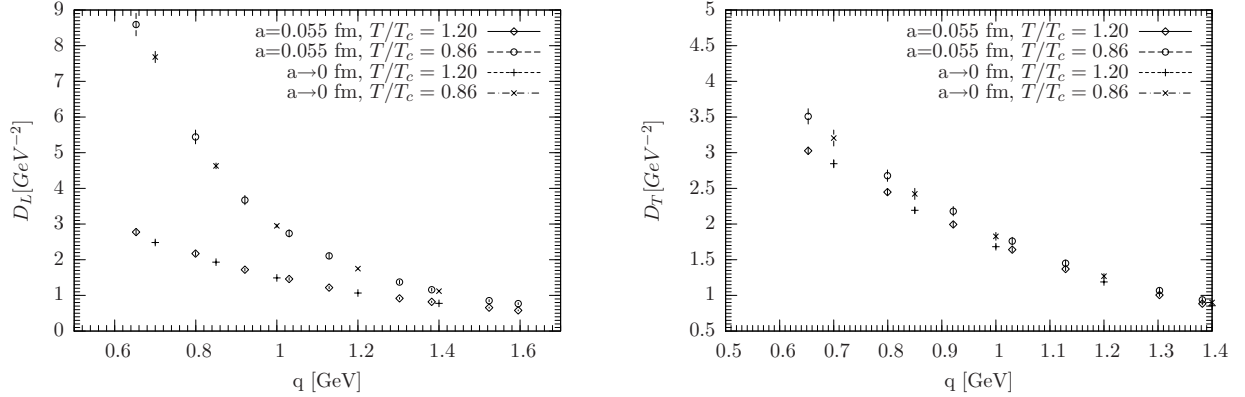


FIG. 13: Comparison of the renormalized propagators $D_L(q)$ (l.h.s.) and $D_T(q)$ (r.h.s.) obtained from the Monte Carlo simulation at $\beta = 6.337$ with some continuum limit extrapolated values.

-
- [1] R. Hagedorn, Nucl.Phys. **B24**, 93 (1970).
 - [2] C. DeTar (2011), 1101.0208.
 - [3] L. von Smekal, A. Hauck, and R. Alkofer, Ann. Phys. **267**, 1 (1998), hep-ph/9707327.

- [4] A. Hauck, L. von Smekal, and R. Alkofer, Comput.Phys.Comm. **112**, 166 (1998), hep-ph/9804376.
- [5] C. D. Roberts and S. M. Schmidt,

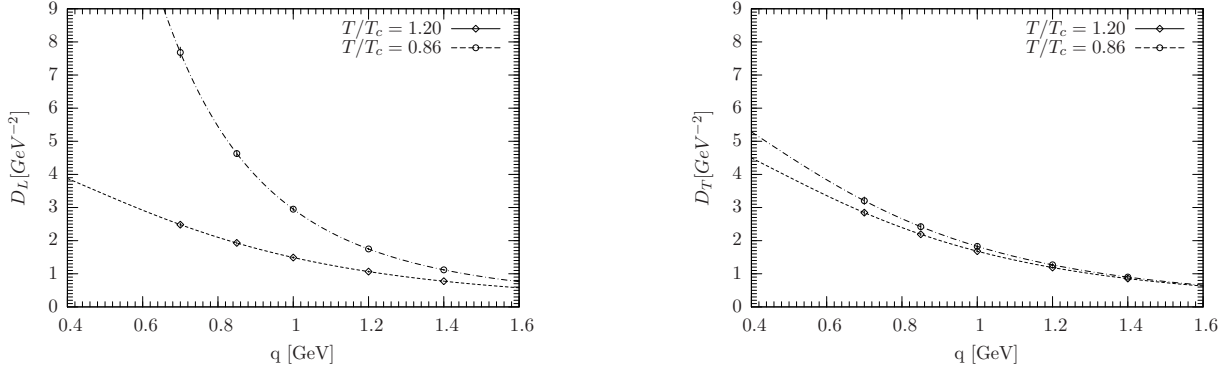


FIG. 14: Continuum extrapolated values of $D_L(q)$ (l.h.s.) and $D_T(q)$ (r.h.s.) together with their respective interpolation curves for two temperature values.

- Prog.Part.Nucl.Phys. **45**, S1 (2000), nucl-th/0005064.
- [6] P. Maris and C. D. Roberts, Int.J.Mod.Phys. **E12**, 297 (2003), nucl-th/0301049.
- [7] H. Gies, Phys.Rev. **D66**, 025006 (2002), hep-th/0202207.
- [8] J. M. Pawłowski, D. F. Litim, S. Nedelko, and L. von Smekal, Phys. Rev. Lett. **93**, 152002 (2004), hep-th/0312324.
- [9] V. N. Gribov, Nucl. Phys. **B139**, 1 (1978).
- [10] D. Zwanziger, Phys. Rev. **D65**, 094039 (2002), hep-th/0109224.
- [11] D. Zwanziger, Phys. Rev. **D69**, 016002 (2004), hep-ph/0303028.
- [12] T. Kugo and I. Ojima, Prog. Theor. Phys. Suppl. **66**, 1 (1979).
- [13] T. Kugo (1995), hep-th/9511033.
- [14] C. S. Fischer, A. Maas, and J. M. Pawłowski, Annals Phys. **324**, 2408 (2009), 0810.1987.
- [15] V. G. Bornyakov, V. K. Mitrjushkin, and M. Müller-Preussker, Phys. Rev. **D81**, 054503 (2010), 0912.4475.
- [16] I. L. Bogolubsky, E.-M. Ilgenfritz, M. Müller-Preussker, and A. Sternbeck, Phys. Lett. **B676**, 69 (2009), 0901.0736.
- [17] U. M. Heller, F. Karsch, and J. Rank, Phys. Lett. **B355**, 511 (1995), hep-lat/9505016.
- [18] U. M. Heller, F. Karsch, and J. Rank, Phys. Rev. **D57**, 1438 (1998), hep-lat/9710033.
- [19] A. Cucchieri, F. Karsch, and P. Petreczky, Phys. Lett. **B497**, 80 (2001), hep-lat/0004027.
- [20] A. Cucchieri, F. Karsch, and P. Petreczky, Phys. Rev. **D64**, 036001 (2001), hep-lat/0103009.
- [21] A. Cucchieri, A. Maas, and T. Mendes, Phys. Rev. **D75**, 076003 (2007), hep-lat/0702022.
- [22] A. Maas, Chin. J. Phys. **34**, 1328 (2010), 0911.0348.
- [23] C. S. Fischer, A. Maas, and J. A. Müller, Eur. Phys. J. **C68**, 165 (2010), 1003.1960.
- [24] A. Cucchieri and T. Mendes (2011), 1105.0176.
- [25] B. Gruter, R. Alkofer, A. Maas, and J. Wambach, Eur.Phys.J. **C42**, 109 (2005), hep-ph/0408282.
- [26] A. Maas, J. Wambach, and R. Alkofer, Eur.Phys.J. **C42**, 93 (2005), hep-ph/0504019.
- [27] J. Braun, H. Gies, and J. M. Pawłowski, Phys. Lett. **B684**, 262 (2010), 0708.2413.
- [28] C. S. Fischer, Phys.Rev.Lett. **103**, 052003 (2009), 0904.2700.
- [29] V. Bornyakov and V. Mitrjushkin (2010), 1011.4790.
- [30] V. G. Bornyakov and V. K. Mitrjushkin (2011), 1103.0442.
- [31] K. Fabricius and O. Haan, Phys.Lett. **B143**, 459 (1984).
- [32] A. Kennedy and B. Pendleton, Phys.Lett. **B156**, 393 (1985).
- [33] N. Cabibbo and E. Marinari, Phys. Lett. **B119**, 387 (1982).
- [34] S. Necco and R. Sommer, Nucl. Phys. **B622**, 328 (2002), hep-lat/0108008.
- [35] G. Boyd, J. Engels, F. Karsch, E. Laermann, C. Legeland, et al., Nucl.Phys. **B469**, 419 (1996), hep-lat/9602007.
- [36] C. Parrinello and G. Jona-Lasinio, Phys. Lett. **B251**, 175 (1990).
- [37] D. Zwanziger, Nucl. Phys. **B345**, 461 (1990).
- [38] T. D. Bakeev, E.-M. Ilgenfritz, V. K. Mitrjushkin, and M. Müller-Preussker, Phys. Rev. **D69**, 074507 (2004), hep-lat/0311041.
- [39] A. Sternbeck, E.-M. Ilgenfritz, M. Müller-Preussker, and A. Schiller, Phys. Rev. **D72**, 014507 (2005), hep-lat/0506007.
- [40] I. L. Bogolubsky, G. Burgio, V. K. Mitrjushkin, and M. Müller-Preussker, Phys. Rev. **D74**, 034503 (2006), hep-lat/0511056.
- [41] I. L. Bogolubsky, V. G. Bornyakov, G. Burgio, E.-M. Ilgenfritz, V. K. Mitrjushkin, and M. Müller-Preussker, Phys. Rev. **D77**, 014504 (2008), 0707.3611.
- [42] A. Nakamura and M. Plewnia, Phys. Lett. **B255**, 274 (1991).
- [43] V. G. Bornyakov, V. K. Mitrjushkin, M. Müller-Preussker, and F. Pahl, Phys. Lett. **B317**, 596 (1993), hep-lat/9307010.
- [44] I. L. Bogolubsky, V. K. Mitrjushkin, M. Müller-Preussker, and P. Peter, Phys. Lett. **B458**, 102 (1999), hep-lat/9904001.
- [45] I. L. Bogolubsky, V. K. Mitrjushkin, M. Müller-Preussker, P. Peter, and N. V. Zverev, Phys. Lett. **B476**, 448 (2000), hep-lat/9912017.
- [46] G. S. Bali, V. Bornyakov, M. Müller-Preussker, and

- F. Pahl, Nucl. Phys. Proc. Suppl. **42**, 852 (1995), hep-lat/9412027.
- [47] G. S. Bali, V. Bornyakov, M. Müller-Preussker, and K. Schilling, Phys. Rev. **D54**, 2863 (1996), hep-lat/9603012.
- [48] I. L. Bogolubsky, V. G. Bornyakov, G. Burgio, E.-M. Ilgenfritz, V. K. Mitrjushkin, M. Müller-Preussker, and P. Schemel, PoS **LAT2007**, 318 (2007), 0710.3234.
- [49] G. Damm, W. Kerler, and V. K. Mitrjushkin, Phys. Lett. **B433**, 88 (1998), hep-lat/9802028.
- [50] A. Sternbeck, E.-M. Ilgenfritz, M. Müller-Preussker, A. Schiller, and I. L. Bogolubsky, PoS **LAT2006**, 076 (2006), hep-lat/0610053.
- [51] A. Sternbeck, PhD thesis, Humboldt-University Berlin (2006), hep-lat/0609016.
- [52] D. B. Leinweber, J. I. Skullerud, A. G. Williams, and C. Parrinello (UKQCD), Phys. Rev. **D60**, 094507 (1999), hep-lat/9811027.
- [53] M. Stingl, Z.Phys. **A353**, 423 (1996), hep-th/9502157.
- [54] A. Cucchieri, T. Mendes, and A. R. Taurines, Phys.Rev. **D67**, 091502 (2003), hep-lat/0302022.
- [55] D. Dudal, J. A. Gracey, S. P. Sorella, N. Vandersickel, and H. Verschelde, Phys. Rev. **D78**, 065047 (2008), 0806.4348.
- [56] D. Dudal, S. Sorella, and N. Vandersickel, Phys.Rev. **D84**, 065039 (2011), 1105.3371.
- [57] A. Cucchieri and T. Mendes, PoS **LAT2007**, 297 (2007), 0710.0412.
- [58] V. Bornyakov, R. Horsley, Y. Nakamura, M. Polikarpov, P. Rakow, et al. (2011), 1102.4461.
- [59] F. Burger, E.-M. Ilgenfritz, M. Kirchner, M. Lombardo, M. Müller-Preussker, et al. (2011), 1102.4530.